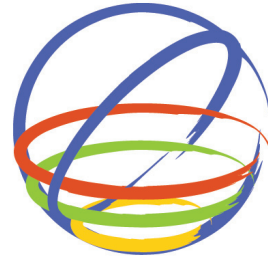


Characteristics of Strong Ground Motions from the Sanriku-Oki Outer-Rise Earthquakes



N. Takai, T. Sasatani & M. Shigefuji

Hokkaido University, Japan

Y. Okazaki

Obayashi Corporation, Japan

15 WCEE

LISBOA 2012

SUMMARY:

A huge interplate earthquake, the 2011 off the Pacific coast of Tohoku Earthquake (Mw9.1), occurred at 14:46, 11 March, 2011. After this, earthquake activity increased around the Sanriku-oki area. The types of aftershocks were not only interplate earthquakes, but also intraslab and outer-rise earthquakes. We gathered data from 5 outer-rise earthquakes in the Sanriku-oki area. First, we calculated pseudo-velocity response spectra for these outer-rise earthquakes. Second, we made spatial distribution maps and we compared these attenuation relationships with our attenuation formulas. The spatial distribution maps showed different features depending on the natural period. In short period ranges, the maps showed strong attenuation of the response at the back-arc side of the volcanic front. Furthermore, we constructed prediction formula of velocity response for short period ranges for each site using regression analysis. Finally, we made a seismic intensity distribution map of the 1933 Showa Sanriku earthquake (Mw8.4).

Keywords: Outer-rise earthquake, Velocity response, Attenuation relationship

1. INTRODUCTION

The attenuation relation of strong earthquake ground motion, which is predictable in wide areas, is important in earthquake engineering. Many experimental attenuation formulas for the estimation of ground motion severity have been developed using regression analysis (e.g., Boore and Joyner, 1982). These formulas are useful in easily predicting strong ground motion and in evaluating newly observed data with simple information: hypocentral distance and magnitude. However, these are based on a homogenous subsurface structure, therefore the predicted values are distributed on a concentric circle. It is now known that a heterogeneous upper mantle structure exists beneath subduction zones such as those in Japan. This structure causes a region of anomalous seismic intensity in northern Japan. For this region, we have to consider the effects of a heterogeneous structure on the attenuation relation. Recently Kanno et al. (2006) proposed correction terms in the prediction equations of PGA, PGV and acceleration response spectra to take account of a heterogeneous structure. However, their prediction equations still assume a single term of inelastic attenuation.

We previously derived prediction formula (Dhakal et al., 2010) for two categories of earthquake, one for interplate earthquakes and another for intraslab earthquakes. In these equations, we divided the source-to-site distance into two distances at the attenuation boundary beneath the volcanic front. The boundary was considered to separate the relatively high Q fore-arc side mantle wedge from the low Q back-arc side mantle wedge.

The 2011 off the Pacific coast of Tohoku Earthquake (Mw9.1) occurred at 14:46, 11 March, 2011. After this, earthquake activity increased around the Sanriku-oki area. The types of aftershocks were not only interplate earthquakes but also intraslab and outer-rise earthquakes.

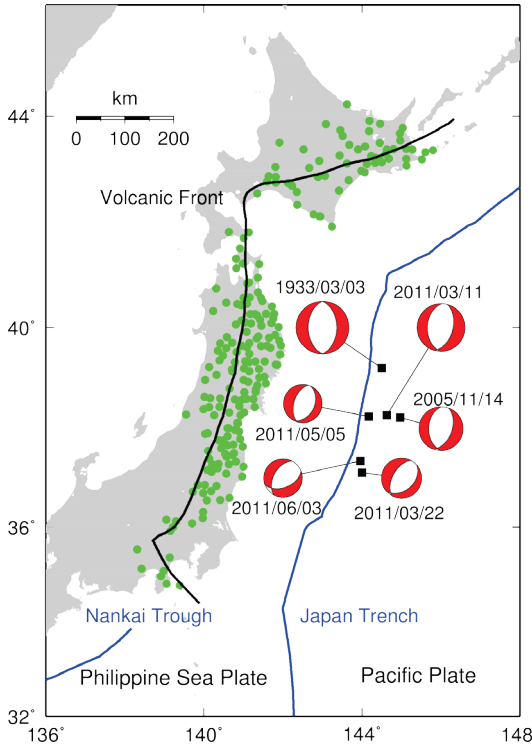


Figure 1. Distribution map of earthquakes and observation stations.
Green points indicate stations used for regression analysis.
CMT solutions of earthquakes are after Global CMT.

Table 1. List of earthquakes used in this study, after Global CMT and Kanamori (1977)*.

Date(GMT)	Time (UTC)	Mw	Depth(km)	No. of Records
2005/11/14	21:38	7.0	18.0	659
2011/03/11	6:26	7.6	21.1	867
2011/03/22	7:18	6.4	12.3	455
2011/05/05	14:58	6.1	13.9	305
2011/06/03	0:05	6.1	20.5	408
1933/03/02 *	17:31	8.4		-

The aftershock (Mw7.6) that occurred at 15:26, 11 March was considered to be an outer-rise earthquake. Moreover, we collected data from 4 other outer-rise earthquakes (Table 1). The epicenters of these 5 outer-rise earthquakes are concentrated within a 100km radius (Figure 1). During these outer-rise earthquakes, large peak ground acceleration values were recorded despite the long epicentral distances and small magnitudes. Near the same area, the 1933 Showa Sanriku earthquake (03 March 1933, Mw8.4) occurred however, the character of its strong ground motion distribution is not yet clear. Thus it is important that the characteristics of strong ground motion from outer-rise earthquakes are grasped with these data.

The outer-rise events were not included in the data used for regression analysis in making our formulas. It should be checked that our prediction formula of intraslab earthquakes can be adapted to these outer-rise events data, because the outer-rise events occur in plates as intraslab earthquakes.

In this study, first we calculated pseudo-velocity response spectra (damping factor $h=0.05$) for these outer-rise earthquakes based on K-NET and KiK-net data. Pacific plate outer-rise earthquakes are typical of high amplitude short period range earthquakes (Sasatani et al. 2012), therefore we discussed response spectra under 1.0 sec. Second, we made spatial distribution maps of response values and attenuation relationships, and compared these attenuation relationships with our attenuation formulas. Furthermore, we constructed a prediction formula of velocity responses in short period ranges for each

site using regression analysis. Finally, we made a seismic intensity distribution map of the 1933 Showa Sanriku earthquake (Mw8.4).

2. DATA

Our target outer-rise earthquakes are the aftershock (Mw7.6) that occurred at 15:26, 11 March, 15 November 2005 (Mw6.0 D=18km), 22 March 2011 (Mw6.4 D=12.3km), 05 May 2011 (Mw6.0 D=12.3km) and 03 June 2011 (Mw6.1 D=19.5km) (Table 1, Figure 1).

We used strong ground motion data obtained from the K-NET and KiK-net of the National Research Institute for Earth Science and Disaster Prevention (NIED) to examine the spatial distribution of velocity responses in north Japan. The number of stations used is listed in Table 1.

We used pseudo-velocity response spectra to compare against our formulas. First, we calculated 5% damped acceleration response time histories with natural periods of $T=0.1, 0.3, 1.0$ sec, of two horizontal components and took the maximum value from their vector sum history. Second, we divided the maximum value by the angular frequency corresponding to the natural period to obtain the pseudo-velocity response.

The strong motion records of the aftershock (Mw7.6) included long period motion before p-wave motion, because of the huge main shock (Mw 9.1). For example, Figure 2 shows the KSRH06 site NS component velocity waveform. We checked the influence of the long period motion to short period response using a low frequency cut filter. Figure 2(a) shows the velocity waveform without filter and Figure 2(b) shows the waveform with filter (0.2 Hz low cut). Long period wave motions are seen in the original wave. Figure 2(c) compares the response spectra for both waveforms. There was no repercussion in response values under 1.0 sec, therefore we calculated response spectra without the filter.

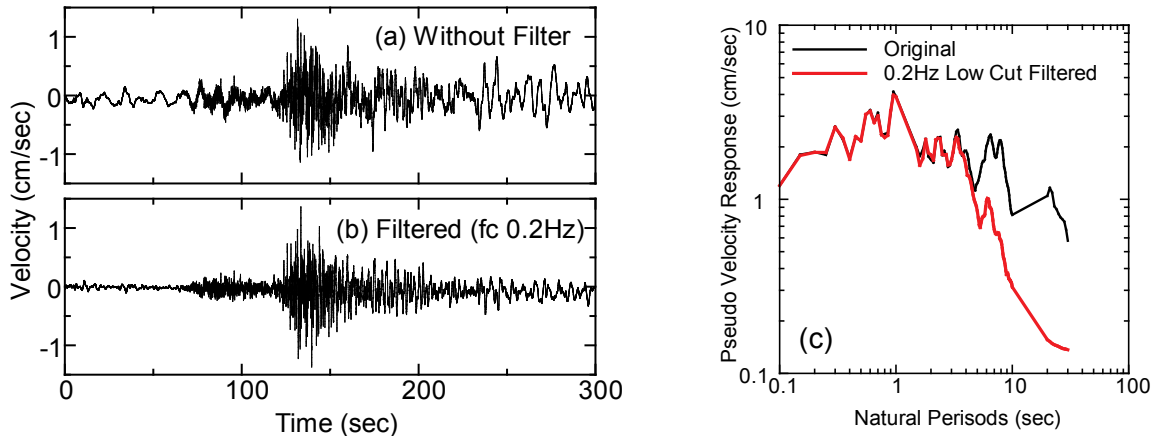


Figure 2. Comparison between velocity waveform and filtered velocity waveform of the KSRH06 station and their pseudo velocity response spectra.

3. METHOD

First, we made distribution maps of response values and compared the response values for each earthquake with the attenuation formula. The attenuation formulas are taking a complex Q structure beneath the Japan arc into account (Dhakal et al., 2010). We divided the hypocentral distance (R) at the volcanic front (V.F.) into the high Q fore-arc side mantle wedge (FAMW) side distance (R_1) and the low Q back-arc side mantle wedge (BAMW) side distance (R_2) in order to consider a heterogeneous Q structure (Fig. 3). The V.F. location in northern Japan is shown in Figures 1 and 4. We use the ratio of the fore-arc side distance to the hypocentral distance, $R_1/(R_1+R_2=R)$, to simply consider the heterogeneous structure.

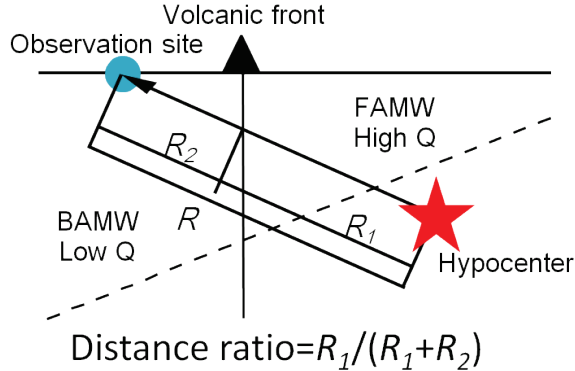


Figure 3. Schematic vertical section of the Japan subduction zone. Definition of distances of R , R_1 and R_2 : R is the distance from the hypocenter to the observation site, R_1 is the distance from the hypocenter to the attenuation boundary, and R_2 is the distance from the attenuation boundary to the observation site. FAMW and BAMW denote the fore-arc side and back-arc side mantle wedges, respectively. Q denotes the quality factor.

Second, we selected 217 sites that observed records of all earthquakes. The epicenters of these 5 outer-rise earthquakes are concentrated within a 100km radius (Figure 1) and the epicenters are a sizeable distance from every site. Therefore, we will check the dependency on magnitude, without serious influence of path effects and site amplification conditions. Through this checking, regression analyses are carried out for each site data and prediction equations for each site constructed.

4. SPATIAL DISTRIBUTION FEATURES OF VELOCITY RESPONSES

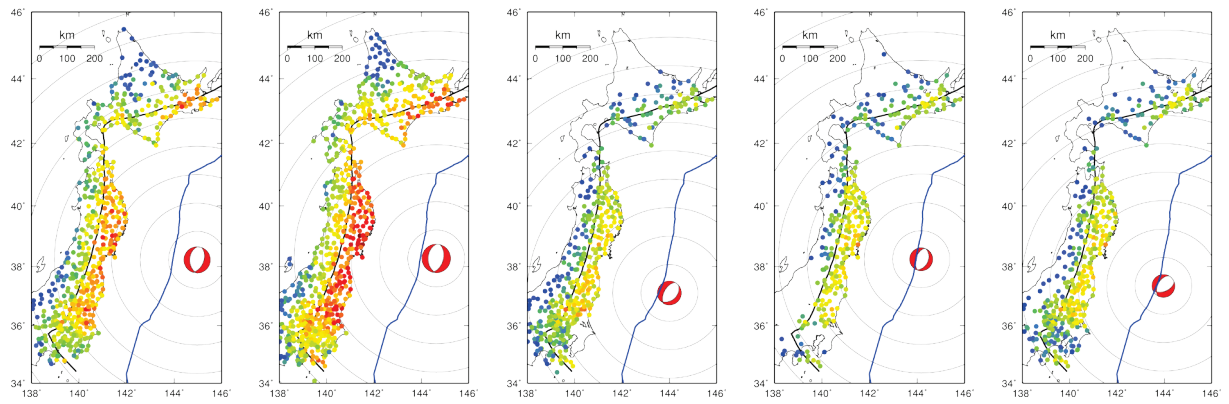
We show the spatial distribution maps for $T=0.1$, 0.3 and 1.0 sec pseudo-velocity responses. Figure 4 shows the distribution maps. These maps are plotted with focal mechanism distributed by the global CMT project. Concentric circles are epicentral distances at intervals of 100km. These maps show different features depending on the period. In Figure 4, the response values increase with period all over northern Japan. In the $T=0.1$ and 0.3 sec maps, the high response values are located along the Pacific Ocean side, that is, along the FAMW. Even though the area on the Pacific Ocean side of Hokkaido Island was far from the epicenter (more than 500km), a large response was observed. On the other hand, in these figures the BAMW have nearly the same low response.

In the $T=1.0$ sec maps in Figure 4, the V.F. has no effects on the spatial distributions, however we can understand that the low land areas were strongly shaken.

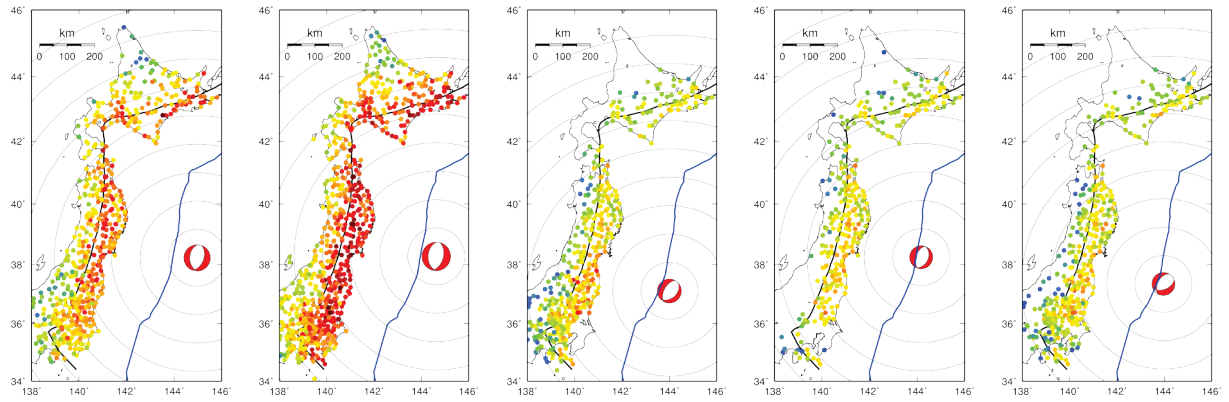
5. ATTENUATION RELATIONS OF PSEUDO VELOCITY RESPONSES

Figure 5 shows the attenuation relations of the pseudo-velocity responses for $T=0.1$, 0.3 and 1.0 sec. The data points are classified by the distance ratio of $R_1/(R_1+R_2)$; the red color represents the site was located on the fore-arc side. The scattering of data points decreases with the period. The $T=0.1$ sec relation shows a large scattering over two orders at distances greater than about 500km, while the $T=1.0$ sec relation shows a considerably smaller scattering. The decay rates also change with the period. We consider that these features result from the seismic source, propagation path and site effects on velocity responses.

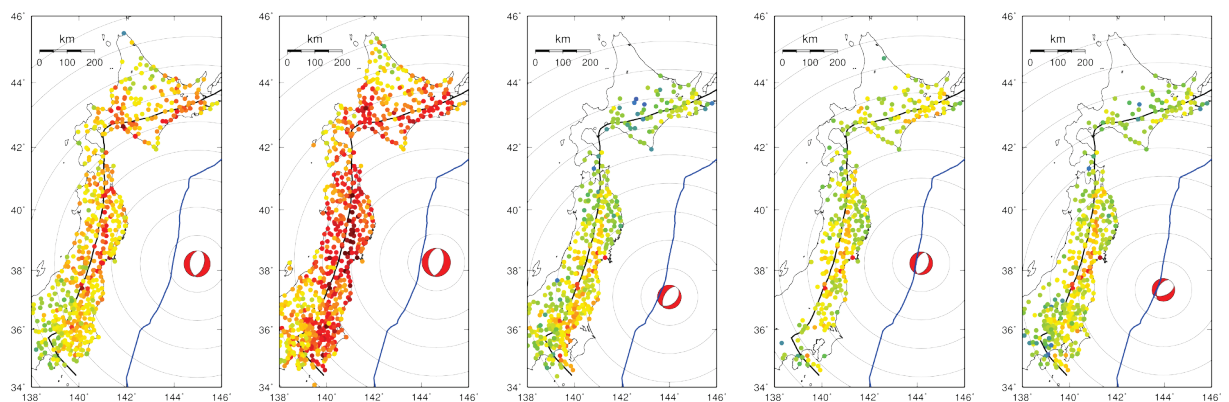
The attenuation curves plotted in Figure 5 are constructed with data that is less than 300km hypocentral distance of the intraslab earthquakes. However, the agreement between the observed values and predicted curve is usually good, as indicated in these figures. It is clearly shown that there is a tendency for the attenuation in particular to vary according to distance ratio. The source characteristics of outer-rise earthquakes are similar to those of intraslab earthquakes (Kawabata et al. 2012). Equally, strong motion distribution characteristics in short period ranges are similar to those of intraslab earthquakes.



(a) $T=0.1\text{sec}$



(b) $T=0.3\text{sec}$



2005/11/14
Mw 7.0

2011/3/11
Mw 7.6

2011/3/22
Mw 6.4

2011/5/5
Mw 6.1

2011/6/3
Mw 6.1

(c) $T=1.0\text{sec}$

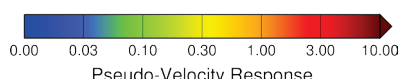


Figure 4. Spatial distribution maps of pseudo-velocity responses for a damping factor of 5% and natural periods of (a) 0.1, (b) 0.3, (c) 1.0 sec.

Solid blue lines represent the Japan trench. The black lines represents the volcanic front.

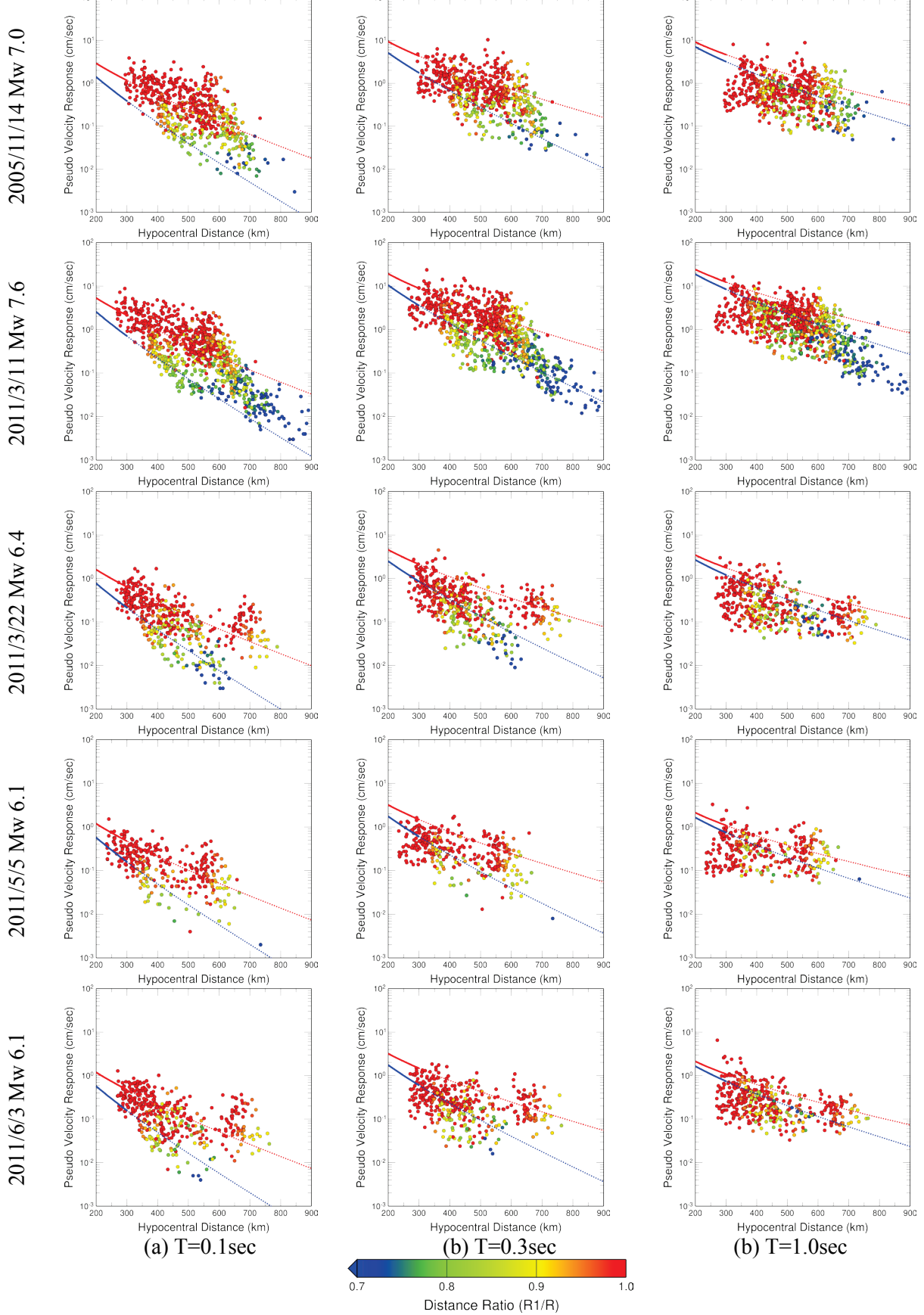


Figure 5. Attenuation relationships of velocity responses for a damping factor of 5% and natural periods of (a) 0.1, (b) 0.3, (c) 1.0sec. The data points are classified by the distance ratio R_1/R . Solid red and blue lines are Dhakal et al.'s formulas for ratios 1.0 and 0.7, and the dashed lines are formulas extended by extrapolation.

6. CONSTRUCTION OF PREDICTION FORMULA FOR EACH SITE

We compared response spectra for each site, for example we show IWTH02 site's spectra in Figure 6. In this figure, it is seen that response values are clearly affected by Mw, and slightly affected by epicentral distance. By the relationship between Mw and response value of T=0.1 sec for the IWTH02 site (Figure 7), we can recognize the possibility of prediction formula construction. However, the spectrum of the nearest 2011/5/5 earthquake (Mw 6.1) is larger than for the 2011/3/22 earthquake (Mw 6.4). Consideration ought to be given to correction for distance attenuation.

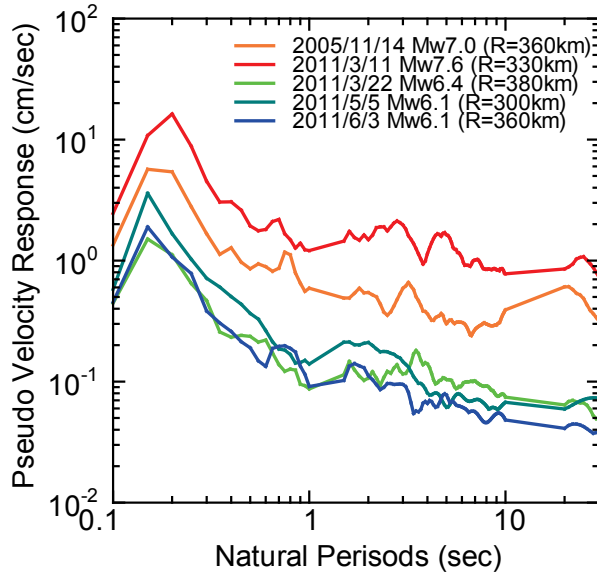


Figure 6. Response spectra of the IWTH02 site. R in legend is mean of epicentral distance.

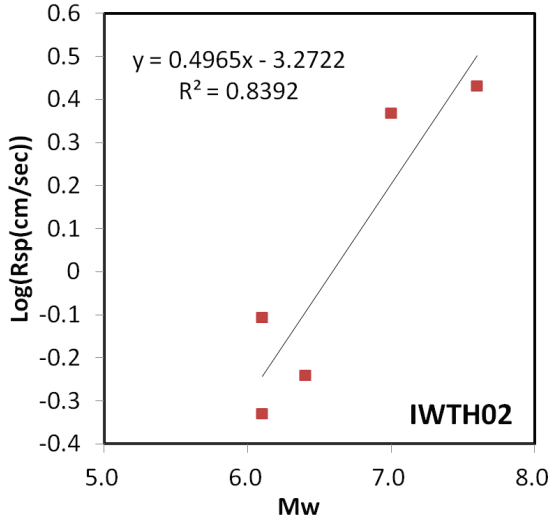


Figure 7. Comparison between response value for T=0.1 sec of the IWTH02 station and Mw. R^2 value represents regression coefficient.

As mentioned above, our prediction formula of intraslab earthquakes explains well the attenuation characteristics of outer-rise earthquake response spectra. Therefore we use the inelastic attenuation term bR of Dhakal et al. (2010) to compensate for attenuation effects. The formula using regression analysis is below.

$$\text{Log}(Rsp) = c + aMw - \log(R) - bR \quad (1)$$

where Rsp is the 5% damped pseudo-velocity response in cm/s for a natural period T in seconds; c and a are the regression coefficients to be determined for each site; Mw is the moment magnitude; R is hypocentral distance; b is the inelastic coefficient of Dhakal et al (2010). Using regression analysis we calculated c, a value for each site.

7. INTENSITY DISTRIBUTION PREDICTION FOR THE 1933 SANRIKU EQ. (M_w 8.4)

We can evaluate the strong ground motion characteristics for a large outer-rise event such as the 1933 Showa Sanriku earthquake with regression coefficients for each of the sites. First, we tried to make a distribution map of response values for $T=0.1, 0.3$ and 1.0 sec (Figure 8).

It can be understood that the coastline sites of the Pacific Ocean have a large response for $T=0.1$ sec and Tohoku inland sites have a large response for $T=0.3$, and 1.0 sec (Figure 8). We speculate that the former features are affected by attenuation path effects and the latter phenomena are affected by deep soft soil deposits around the Kitakami river basin region.

For the 1933 Showa Sanriku earthquake, we have only the intensity distribution map from the Japan Meteorological Agency (JMA). Our results produce only response spectra, however we can calculate JMA intensity with acceleration response spectra (Sakai et al., 2002). We calculated JMA intensity with average values of 0.1-1.0 sec and plotted the results (Figure 9), then compared these with the JMA observed map. As the calculation method for JMA intensity is different today from in those days, the direct comparisons of the values are not important, but the comparison of distribution tendency is meaningful. It is same pattern with high intensity distributed in east area of Hokkaido. There is not a high intensity distribution area in the centre of Tohoku in the observed map. We conjecture that the cause of this phenomenon depends on the resolution of the observed intensity distribution map.

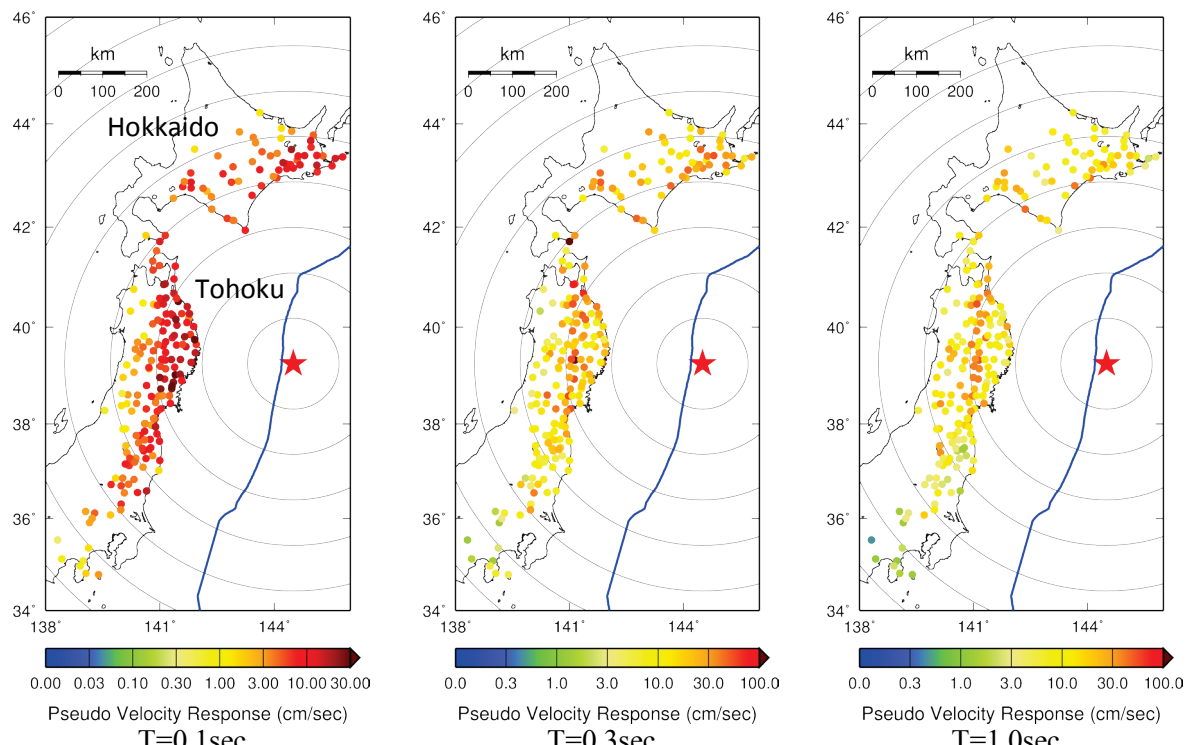
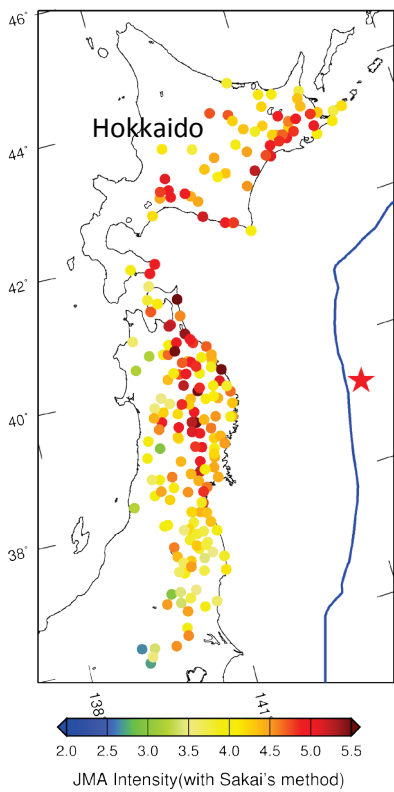
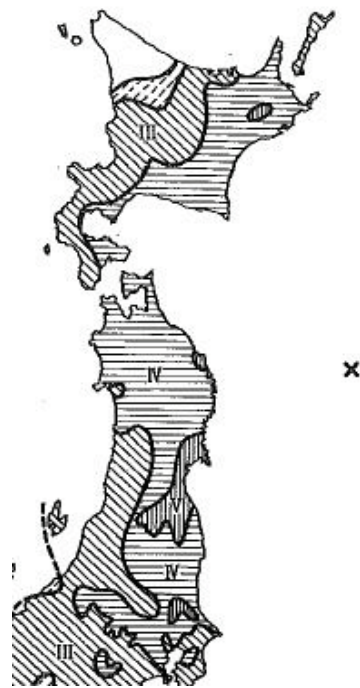


Figure 8. Spatial distribution maps of predicted pseudo-velocity responses for a damping factor of 5% on the 1933 Showa Sanriku earthquake (M_w 8.4).



(a) Predicted JMA intensity



(b) Observed JMA intensity (Usami, 2003).

Figure 9. Spatial intensity distribution maps of the 1933 Showa Sanriku earthquake (Mw 8.4).

8. CONCLUDING REMARKS

In this study, first we calculated pseudo-velocity response spectra (damping factor $h=0.05$) for 5 outer-rise earthquakes based on K-NET and KiK-net data. Second, we made spatial distribution maps of response values and attenuation relationships. Furthermore, we compared these attenuation relationships with our attenuation formulas. In short period ranges, the relationships between velocity response and hypocentral distance were well expressed with our prediction formulas of intraslab earthquakes.

We constructed prediction formula of velocity responses in short period ranges for each site using regression analysis. We made a JMA seismic intensity distribution map of the 1933 Showa Sanriku earthquake (Mw8.4), and compared it with the observed JMA intensity map. The predicted map explains the tendency of distribution pattern well.

By taking these findings into account, we shall try to upgrade the prediction method of a wide-band and wide distance, high-precision response spectrum for a large earthquake.

ACKNOWLEDGEMENT

The strong ground motion records are collected by the National Research Institute for Earth Science and Disaster Prevention (NIED, <http://www.kyoshin.bosai.go.jp/kyoshin/>). We used CMT solutions from the Global CMT project. We gratefully appreciate the work from these groups. Some figures were made by GMT (Generic Mapping Tools, Wessel and Smith, 1991).

REFERENCES

- Boore, D.M, and Joyner W.B., (1982), The empirical prediction of ground motion, *Bull. Seism. Soc. Am.*, Vol. 72,

No. 1, S43-S60.

- Kanamori, H., (1977), The energy release of great earthquakes., *J. Geophys. Res.*, 82, 2981-2987.
- Kanno T., Narita A., Morikawa N., Fujiwara H., and Fukushima Y., (2006), A New Attenuation Relation for Strong Ground Motion in Japan Based on Recorded Data, *Bull. Seism. Soc. Am.*, Vol. 96, No. 3, 879–897.
- Kawabata W., Sasatani T., Takai N. and Shigefuji M., (2012), Short-Period Source Characteristics of a Great Earthquake Doublet in the Central Kurile Islands., *15th WCEE proceedings (in press)*.
- Dhakal Y. P., Takai N. and Sasatani T., (2010), Empirical analysis of path effects on prediction equations of pseudo-velocity response spectra in northern Japan. *Earthquake Engng Struct. Dyn.*, 39, 443–461.
- Sakai Y., Koketsu K., Kanno T., (2002), Proposal of the destructive power index of strong ground motion for prediction of building damage ratio. *J. Struct. Constr. Eng., AJJ*, 555, 85-91.
- Sasatani T., Takai N., Shigefuji M., Kawabata W., Okazaki Y. and Miyahara Y., (2012), Source Characteristics of Large Outer Rise Earthquakes in the Pacific Plate., *15th WCEE proceedings (in press)*.
- Usami T., (2003), Materials for comprehensive list of destructive earthquakes in Japan (latest edition), University of Tokyo Press.
- Wessel, P. and Smith W. H. F., (1991), Free software helps map and display data, *EOS Trans. AGU*, 72, 441.